An Adjustable Single Degree-of-Freedom System to Guide Natural Walking Movement for Rehabilitation

Brandon Y. Tsuge*
Graduate Student Researcher
Email: btsuge@uci.edu

J. Michael McCarthy
Professor, ASME Fellow
Robotics and Automation Laboratory
Department of Mechanical Engineering
University of California
Irvine, California 92697
Email: jmmccart@uci.edu

This paper presents a linkage system designed to guide a natural ankle trajectory with the corresponding foot orientation. A six-bar linkage was designed to coordinate the joint angles of an RR chain (R denotes a revolute or hinged joint) that models the leg to achieve the desired ankle trajectory. The design is shown to be adjustable to meet a range of trajectories obtained in an individual's normal gait. Control of the foot position is obtained using a cam-driven parallel chain that has the same input as the six-bar linkage. The result is a one degree of freedom system that guides a natural walking movement of the leg and foot. A solid model of the complete device is presented.

1 Introduction

Robotic systems are finding increased use to support treadmill-based rehabilitation for stroke patients and those with spinal cord injuries. These systems attached actuators to a patient's legs that are programmed to provide a desired leg movement. These systems expand the capability of the one degree-of-freedom *Gait Trainer* [1], which was designed to move the users foot, to include movement of the knee and hip. Examples are the pneumatically operated gait orthosis, POGO [2], the pneumatically powered gait orthosis, PPGO [3], and the pneumatically actuated robotic system [4]. Also see the review article by Koceska and Koceski [5].

The paper presents the design of a mechanical system that provides support for natural movement of the hip, knee, and ankle with a single actuator. The design of this device applies recent research on an innovative six-bar linkage matched to the dimensions of the user that coordinates the hip and knee movements to achieve a natural trajectory for the ankle by Tsuge et al. [6]. A parallel cam-mechanism driven by the same input controls the angle of the foot through this trajectory. The result is a compact mechanical system that provides a repeatable natural leg movement for treadmill rehabilitation. An important feature of the design is that it also provides an adjustment that can vary the ankle trajectory to provide natural variations to the stepping movement.

2 Literature Review

Mechanical systems for walking rehabilitation appear as either over-ground systems or treadmill systems. Over-ground systems are exoskeletons that include mechanical braces and actuators under computer control such as the Berkeley Exoskeleton [7, 8] and the MindWalker project [9]. More common are such treadmill systems that are designed for use in a dedicated therapy room under the supervision of a physical therapist. For example, the pelvic assist manipulator, PAM, [10], includes a body-weight support and manipulates the hip of the user on the treadmill. The Active Leg Exoskeleton, ALEX, [11–13] includes body-weight support and independently actuates the hip and knee joints with the ankle supported by a spring-loaded shoe.

Other treadmill systems include the driven gait orthosis, DGO, which provides a lower limb exoskeleton that is actuated at the knee and the hip with a DC motors. The Ambulation-assisting Robotic Tool for Human Rehabilitation, ARTHuR, uses two linear actuators to drive a linkage attached to the angle to manipulate the lower leg on a treadmill [14]. The LOKOMAT [15], and the Lower Extremity Powered Exoskeleton, LOPES [16], provide actuators that

*Address all correspondence related to ASME style format and figures to this author.

therapeutic control the hip and the knee joints. Several systems have been developed for separate actuation of the ankle and foot for treadmill gait rehabilitation by Agrawal et al. [17], Sawicki and Ferris [18], and Kinnaird and Ferris [19].

Our goal is a single degree-of-freedom system that provides natural motion to the hip, knee, angle and foot. Central to this design is a six-bar linkage that includes an RR chain that matches the upper and lower leg dimensions of the user. The ankle trajectory is used to define the movement of this RR chain and the dimensions of the six-bar linkage ensure the movement has one degree-of-freedom. Other systems that provide a one degree-of-freedom ankle trajectory are the Klann six-bar linkage [20], and Jansen eight-bar linkage [21, 22]. There are other single degree-of-freedom, planar linkages that create walking motions developed for biped robots, applications [23, 24]. However, these linkages do not match the natural trajectory of the human ankle and do not control foot orientation.

The synthesis of the six-bar linkage that guides the RR chain to achieve the natural ankle trajectory combines the synthesis theory of six-bar function generators and optimization theory [6]. The cam-driven parallel linkage [25] is introduced to actuate the foot orientation around the ankle in parallel with the six-bar linkage that controls hip and knee.

Finally, local optimization of the six-bar linkage using a greedy search strategy provides designs for each of a set of naturally varying ankle trajectories. The clustering of these designs around a specific set of dimensions yields an adjustment that guides the ankle joint through the natural variation of its trajectory. The result is a compact, simple and innovative linkage system to support treadmill rehabilitation.

3 Natural Ankle Trajectories

In order to design the six-bar linkage that controls the hip and knee to achieve a natural trajectory for the ankle, we begin by obtaining motion capture data of treadmill walking by healthy volunteer. The data was collected using the Vicon MX three dimensional motion capture system by Nina Robson in the Human Interactive Robotics Lab at the California State University, Fullerton, Figure 1.

Motion capture data was collected from markers at the hip, knee, ankle, and toe as the user walked on a treadmill. The ankle data consists of 23 trajectories ranging from 199 to 210 points, Figure 2. The dimensions of the RR chain that model the upper lower leg were obtained from the hip, knee and ankle trajectories.

Because the six-bar linkage is to be designed to attach to the hip, the coordinates of the ankle trajectory data points were transformed to a coordinate system in the hip. This yielded the 23 different trajectories shown in Figure 3, which are the basis for the design of our gait system.

4 Six-Bar Linkage Mechanism for the Ankle Trajectory

The synthesis procedure follows that Tsuge et al. [6], called homotopy directed optimization. This consists of using a combination of homotopy and optimization methods to

Fig. 1: Attached marker locations

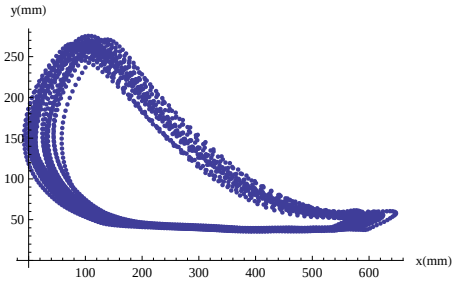

Fig. 2: Ankle trajectories obtained from the Vincon MX motion capture system.

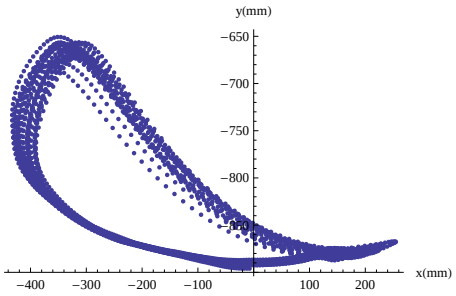

Fig. 3: Ankle trajectories transformed to a coordinate system in the user's hip.

design a Stephenson III, six bar linkage. Homotopy continuation is used to solve the six-bar path synthesis problem for 7 precision points. The resulting linkage solutions are then used as a start population to minimize an objective function that utilizes 60 precision points. The notation for the various joint parameters, the relative link angles are shown in Figure 4. The points $\mathbf{A}, \mathbf{B}, \mathbf{C}, \mathbf{D}, \mathbf{F}, \mathbf{G}$, and $\mathbf{H}$ are the joint coordinates in the fixed frame and ψ, ρ, ϕ, μ, and θ are relative angles of each of the links relative to a starting linkage position. In the context of using this particular linkage topology for the purpose of an exoskeleton, the point $\mathbf{B}, \mathbf{F}$, and $\mathbf{P}$ are modeled as the hip, knee, and ankle joint respectively. The synthesis algorithm requires that a set of ankle points for $\mathbf{P}$ be defined. The value of $\mathbf{B}$ was set to be at the origin for the simplicity.

The data points for the input $\mathbf{P}$ was collected from motion capture data. This data contained coordinates of the ankle during several gait cycles. The first set of ankle coordinates is shown in Figure 5. These are data points are relative to the hip joint. A B-spline [26] was used to repre-

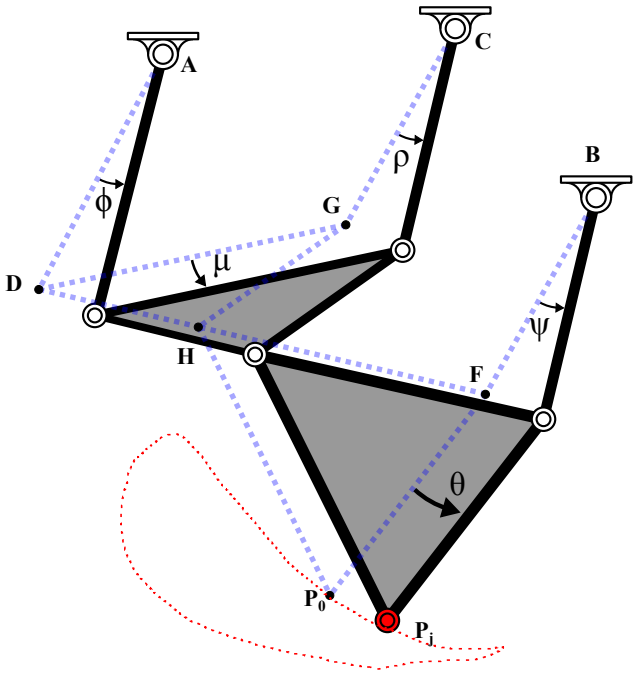

Fig. 4: Stephenson III Six-Bar Linkage

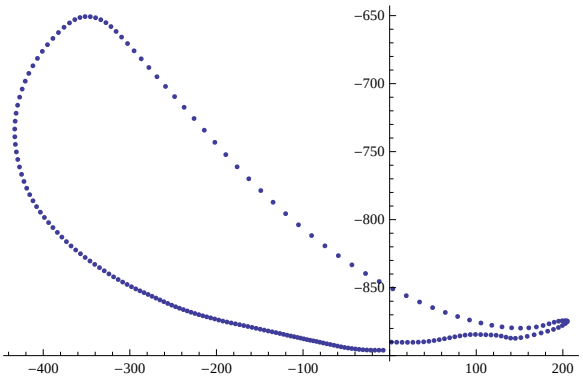

Fig. 5: Ankle Trajectory of a Single Gait Cycle Relative to the Hip Joint

sent the equation of the curve that goes through these data points. From this equation, 7 data points are selected for the homotopy component of the synthesis procedure, and 60 data points were selected for the optimization component. Figure 6 shows a plot of these 60 data points and Figure 7 plots the 7 points required for the homotopy solution.

4.1 Objective Function

The objective function is derived from the loop equations of the six-bar linkage:

$$
\begin{aligned}
&Q_k(D-A) = -U_k(H-D) - T_k(P_0-H) + (P_k-A),\\
&\bar{Q}_k(\bar{D}-\bar{A}) = -\bar{U}_k(\bar{H}-\bar{D}) - \bar{T}_k(\bar{P}_0-\bar{H}) + (\bar{P}_k-\bar{A}),\\
&R_k(G-C) = -U_k(H-G) - T_k(P_0-H) + (P_k-C),\\
&\bar{R}_k(\bar{G}-\bar{C}) = -\bar{U}_k(\bar{H}-\bar{G}) - \bar{T}_k(\bar{P}_0-\bar{H}) + (\bar{P}_k-\bar{C}),\\
&k = 1,\ldots,N_P-1, \qquad (1)
\end{aligned}
$$

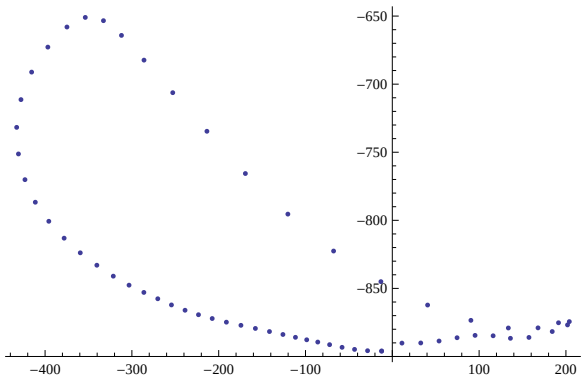

Fig. 6: Set of 60 Precision Points Derived from a B-Spline for the optimization problem

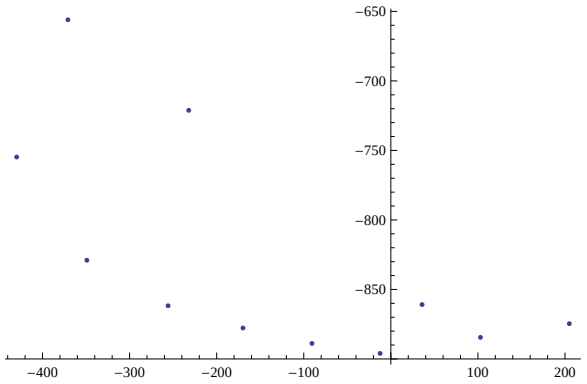

Fig. 7: Set of 7 Precision Points Derived from a b-Spline for homotopy continuation

where (A,C,D,G,H) are the joint parameters and Q,U,T, and R are the relative rotations of the particular link. These variables are in complex form and their complex conjugates are denoted by a bar.

The rotations, Q_k and R_k were eliminated by multiplying the complex conjugate equations.

$$
\begin{aligned}
&|D-A|^2 = |U_k(H-D) + T_k(P_0-H) - (P_k-A)|^2,\\
&|G-C|^2 = |U_k(H-G) + T_k(P_0-H) - (P_k-C)|^2,\\
&k = 1,\ldots,N_P-1, \qquad (2)
\end{aligned}
$$

resulting in k sets of two linear equations. The variables U_k and $\bar{U}_k$ are unknown.

Additional parameters are introduced to solve this system of equations,

$$
\begin{aligned}
&a = a_x + ia_y = H-D\\
&b_k = b_{xk} + ib_{yk} = T_k(P_0-H) - P_k + A\\
&c = c_x + ic_y = H-G\\
&d_k = d_{xk} + id_{yk} = T_k(P_0-H) - P_k + C\\
&f = f_x + if_y = D-A\\
&g = g_x + ig_y = G-C. \qquad (3)
\end{aligned}
$$

Next, the substitution of (3) into (2) results in

$$U_k a\bar{b}_k + \bar{U}_k \bar{a} b_k = f\bar{f} - a\bar{a} - b_k\bar{b}_k,$$
$$U_k c\bar{d}_k + \bar{U}_k \bar{c} d_k = g\bar{g} - c\bar{c} - d_k\bar{d}_k, \quad k = 1,\ldots,N_P-1. \quad (4)$$

Each of these can be solved using Cramer's rule:

$$U_k = \frac{\begin{vmatrix} f\bar{f} - a\bar{a} - b_k\bar{b}_k & \bar{a}b_k \\ g\bar{g} - c\bar{c} - d_k\bar{d}_k & \bar{c}d_k \end{vmatrix}}{\begin{vmatrix} a\bar{b}_k & \bar{a}b_k \\ c\bar{d}_k & \bar{c}d_k \end{vmatrix}}, \bar{U}_k = \frac{\begin{vmatrix} a\bar{b}_k & f\bar{f} - a\bar{a} - b_k\bar{b}_k \\ c\bar{d}_k & g\bar{g} - c\bar{c} - d_k\bar{d}_k \end{vmatrix}}{\begin{vmatrix} a\bar{b}_k & \bar{a}b_k \\ c\bar{d}_k & \bar{c}d_k \end{vmatrix}},$$
$$k = 1,\ldots,N_P-1. \quad (5)$$

The normality condition, $U_k\bar{U}_k = 1$, results in the construction of the objective function, that has the design variable vector $\mathbf{r} = (A,C,D,G,H)$. This objective function is

$$F(\mathbf{r}) = \sum_{i=1}^{N_P-1} U_k\bar{U}_k - 1 = \sum_{i=1}^{N_P-1} \sin^2\mu_k + \cos^2\mu_k - 1, \quad (6)$$

The results of gradient optimization using this objective function were then evaluated to ensure performance and practical dimensions. This yielded six design candidates described in Tsuge et al. [6]. A design refinement strategy was used to eliminate hyper-extension.

4.2 Six-Bar Linkage Design Refinement

We introduced a $\pm$10mm zone was identified around each of the joint locations for this linkage design. Random points within these zones were used to generate an initial population of 50 linkages that are close to the current design. Gradient optimization and performance verification yielded 12 new linkage candidates.

In order measure the similarity between these linkage candidates, we used a clustering formula to measure that distance between linkage joints of a selected design, $L_{\text{ref}} = (\mathbf{A},\mathbf{B},\mathbf{C},\mathbf{D},\mathbf{F},\mathbf{G},\mathbf{H})_{\text{ref}}$ and the remaining designs, given by,

$$V_j = \sqrt{L_{\text{ref}} - L_j}, j = 1,\ldots,11. \quad (7)$$

If we divide this variation by $\sqrt{14} = 3.74$, two coordinates for seven joints, we obtain the average difference between the joint coordinates of the linkages relative to the reference linkage.

The largest variance from the existing design among the 12 solutions was 51.3, which is an average difference of 13.7 mm in the coordinates of the linkage designs. Figure 9 shows one of these new designs that achieves the desired trajectory without hyper-extension of the knee.

4.3 Design for Each Trajectory

This design procedure was applied to each of the 23 gait trajectories shown in Figure 3. The result was 148 designs,

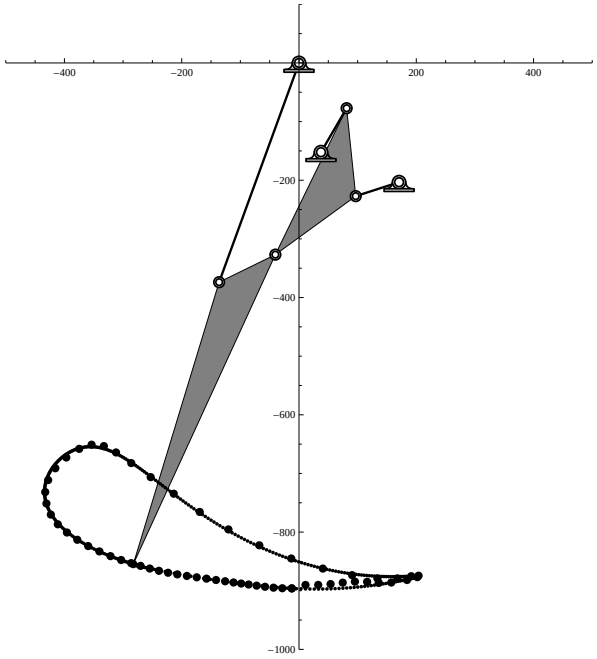

Fig. 8: Optimized Walking Linkage Solution for the Ankle Trajectory

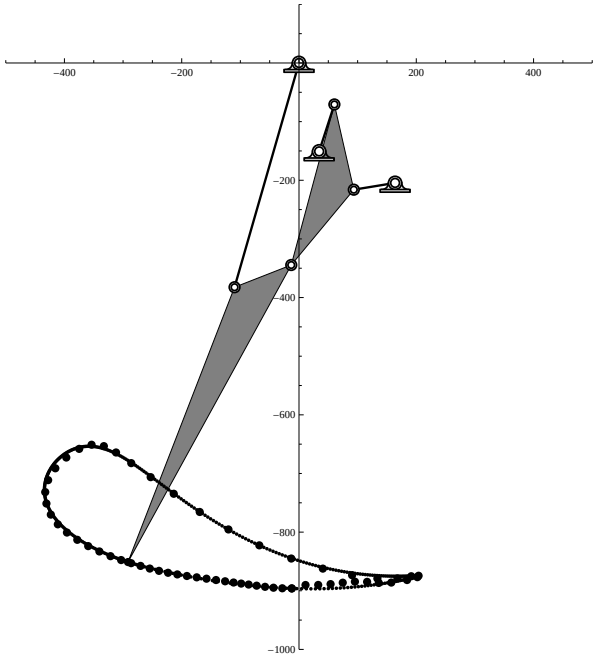

Fig. 9: Optimized walking linkage solution found with design refinement.

which when evaluated using clustering formula (7), showed that that they were all similar to the linkage design for the first trajectory. The largest variance was 100.4, which is an average difference in coordinates of 26.8mm.

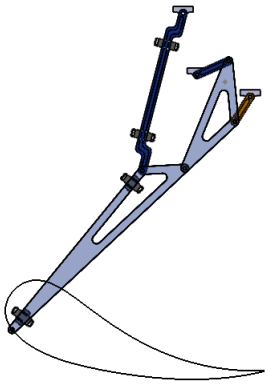

Fig. 10: A solid model of the six-bar linkage for the ankle trajectory obtained from homotopy directed optimization with design refinement.

5 Parallelogram Mechanism for the Foot Orientation Angle

The next component of the walking exoskeleton device is the linkage used to manipulate the orientation angle of the foot. The mechanism used to move the foot angle utilizes of combination of parallelogram linkages, a slider crank linkage, and a cam profile. The parallelogram linkage is required in order to move the foot without affecting the six-bar linkage from the previous section. This slider crank is used to change move the angle of the parallelogram linkage. A diagram of these components is shown in Figure 11. A parallelogram linkage and slider crank mechanism attached to the points **B**, **F**, and **P** of the six bar linkage.

The slider crank is defined by the dimensions l_1 and l_2 and the angles $\alpha_1, \alpha_2, \alpha_3$ and α_4, Figure 11. Since angle of the foot, relative to the x-axis ranges from -79.84° to 15.36° the offset angle α_3 is set to 18° in order to ensure that the joint connecting the links l_1 and l_2 does not pass through the slider axis.

In order to actuate this linkage, we use a cam to moves the slider to achieve the function, $s(\alpha_1)$. The values of α_1 are determined from the motion capture data. The loop equations for the slider crank define the angles α_2 and α_4 [27] as,

$$\alpha_2 = \arcsin\left(\frac{\sin(\alpha_3-\alpha_1)l_1}{l_2}\right), \; \alpha_4 = 360 - (\alpha_3-\alpha_1) - \alpha_2. \tag{8}$$

The value for $s(\alpha_1)$ is given by

$$s(\alpha_1) = \frac{l_1 \sin\alpha_4}{\sin\alpha_2}. \tag{9}$$

The displacement function $s(\alpha_1)$ and the choice of a 10mm roller follower yields the cam profile, [28]. The calculated cam profile is shown in Figure 12. This six-bar linkage that controls the ankle trajectory with the cam-driven parallelogram linkages for the foot orientation is shown in Figure 13.

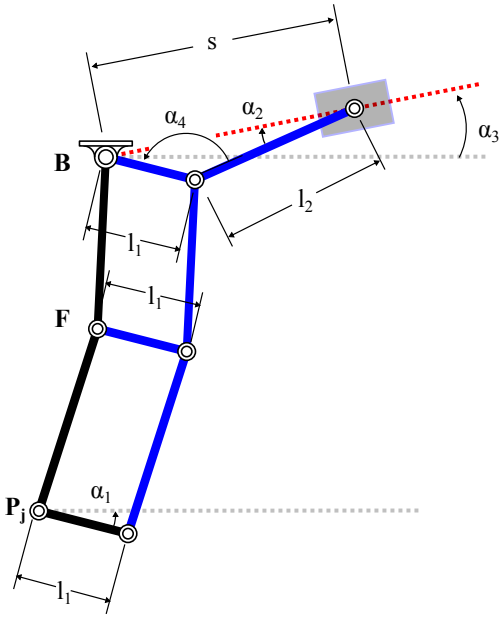

Fig. 11: The foot orientation is controlled by a cam-driven parallelogram linkage.

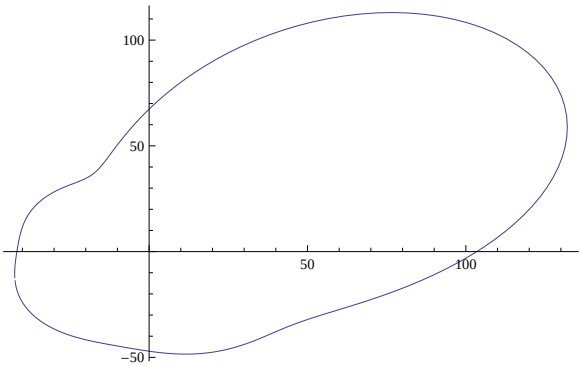

Fig. 12: Cam Profile used to Actuate the Slider Crank Mechanism

Table 1: Coordinates and link lengths of the adjustable drive link **AB** and pivot **A**.

Joint	Coordinates	Link Length
$\mathbf{A}_{\text{design}}$	$(163.9, -204.5)$	71.4mm
$\mathbf{A}_{\text{upper}}$	$(167.9, -198.5)$	72.1mm
$\mathbf{A}_{\text{lower}}$	$(167.9, -194.5)$	70.5mm

6 Adjustment for Variations in Trajectories

The similarity of the linkage designs for each of the 23 trajectories lead us to seek and adjustment to the six-bar linkage that will cover the variation in trajectories. Table **??** provides, the adjustment to the coordinates of the joint **A** and the input link **AB** that allows the ankle trajectory to vary between the extremes shown in Figure **??**.

The result is an adjustment to fixed pivot **A** and the driving link **AB** that allows variation of the ankle trajectory

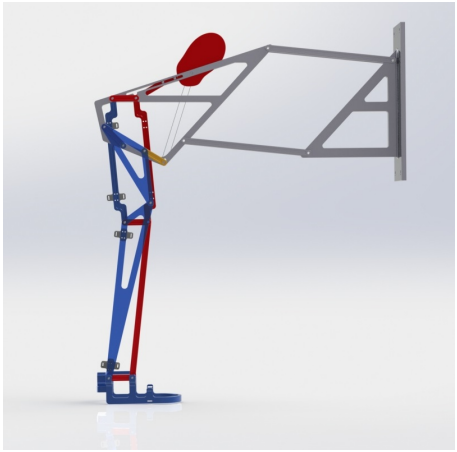

Fig. 13: Assembly of the six-bar linkage that guides the ankle trajectory with the cam-driven parallelogram linkage that controls the foot orientation.

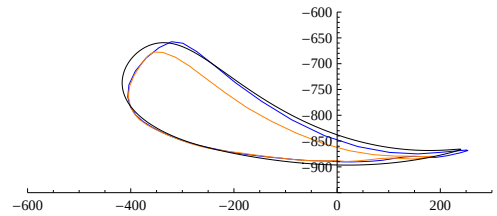

(a) Six-bar linkage trajectory (black) near upper ankle trajectory (blue).

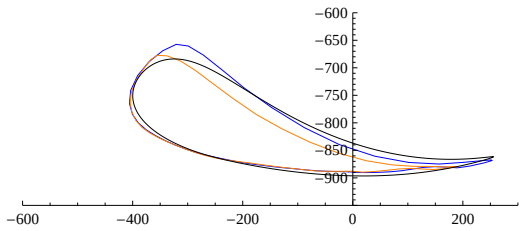

(b) Six-bar linkage trajectory (black) near the lower ankle (orange).

Fig. 14: An adjustment to joint **A** introduces a variation of the ankle trajectory between two extremes, shown in blue and orange.

through the 23 trajectories obtained from the motion capture data.

For convenience, we refer to this one degree-of-freedom mechanism, that combines the adjustable six-bar linkage with the cam-driven parallelogram linkage, the UCI Gait Mechanism.

7 Solid Model of the UCI Gait Mechanism

Figure 15 shows the rendered solid model of the UCI Gait Mechanism mounted, for use on a treadmill. The wall-mounted parallelogram linkage supports the trunk of the user. The six-bar linkage elements are blue in color and the cam mechanism and parallelogram, foot orientation, linkage is colored in red. Figure 16 how the upper portion of the

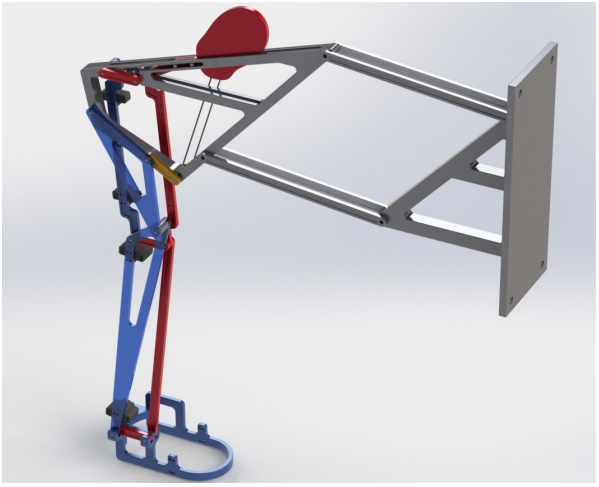

Fig. 15: Solid Model of the UCI Gait Mechanism

Fig. 16: Slider-crank mechanism that is actuated by a cam.

device houses the slider crank can cam mechanism and how the rotation of the input link of the six-bar linkage can be coupled to the cam, using a belt. Figure 18 shows how the parallelogram mechanism attaches to the six-bar linkage, and ultimately moves the foot.

It is also shown how there are black brackets that are attached to the linkage. These are the attachment points that secure the user's leg to the mechanism. The brackets secure rigidly to the six-bar linkage components that have the same dimensions as the user's leg; these brackets have slotted holes so that straps can be threaded through. The straps are the components that are intended to secure the leg to the linkage. Lastly, figure 19 show the foot bracket. This bracket also has slotted holes for straps to fix the foot.

8 Conclusion

This paper describes a single degree-of-freedom rehabilitation system, that we call the UCI Gait Mechanism. This system has been designed to guide the trajectory of a human leg so that it follows a natural walking movement. It consists of an adjustable six-bar linkage that guides the ankle through a natural variation of trajectories, and a cam driven parallelogram linkage that controls the foot orientation.

This single degree-of-freedom gait mechanism provides internal forces that support the users leg so that it achieves a

Fig. 17: The parallelogram mechanism attaches to the six-bar linkage in order to control the foot orientation angle.

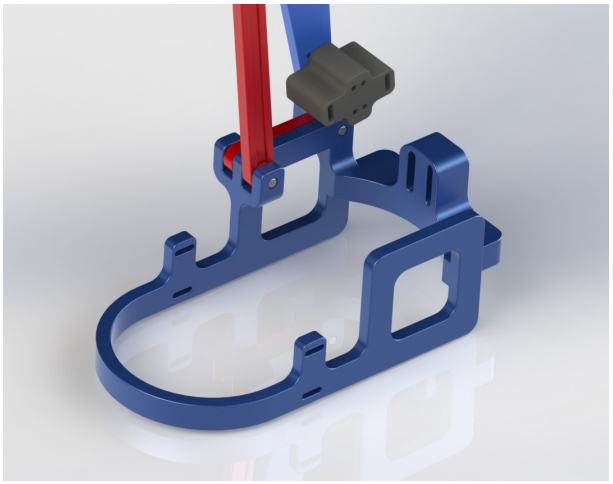

Fig. 18: Foot bracket with slotted holes for straps that will secure the user's foot in place.

natural walking movement. It can be used to move the user's leg or have the user's leg drive a resistance, with or without gravity loading on the leg.

A complete solid model of the UCI Gait Mechanism is shown to illustrate its design and how the device would be used.

Acknowledgements

This material is based upon work supported by the National Science Foundation under Grant No. CMMI 1066082.

References

[1] Hesse, S., and Uhlenbrock, D., 2000. "A mechanized gait trainer for restoration of gait". *Journal of Rehabilitation Research and Development,* **37**(6), November/December.

[2] Aoyagi, D., Ichinose, W. E., Harkema, S. J., Reinkensmeyer, D. J., and Bobrow, D. J., 2007. "A robot and control algorithm that can synchronously assist in naturalistic motion during body-weight-supported gait training following neurologic injury". *IEEE Transactions on Neural Systems and Rehabilitation Engineering,* **15**(3), pp. 387–400.

[3] Zhou, S., and Song, J., 2011. "Design and control of pneumatically-powered gait orthosis". In Proceedings of the 5th International Conference on Bioinformatics and Biomedical Engineering, IEEE.

[4] Koceska, N., Koceski, S., Zobel, P. B., and Durante, F., 2011. "Gait training using pneumatically actuated robot system". In *Advances in Robot Navigation*, P. A. Barrera, ed. InTech.

[5] Koceska, N., and Koceski, S., 2013. "Review: Robot devices for gait rehabilitation". *International Journal of Computer Applications,* **62**(12), January.

[6] Tsuge, B. Y., Plecnik, M., and McCarthy, J. M., 2015. "Homotopy directed optimization to design a six-bar linkage for a lower limb with a natural ankle trajectory". *Submitted to the Journal of Mechanisms and Robotics*(JMR-15-1225).

[7] Zoss, A. B., Kazerooni, H., and Chu, A., 2006. "Biomechanical design of the berkeley lower extremity exoskeleton (bleex)". *IEEE/ASME Transactions on Mechatronics,* **11**(2), April, pp. 128–138.

[8] Strickland, E., 2012. "Good-bye wheelchair". *IEEE Spectrum*, January.

[9] Gancet, J., Ilzkovitz, M., Motard, E., Nevatia, Y., Letier, P., Weerdt, D. D., Cheron, G., Hoellinger, T., Seetharaman, K., Petieau, M., Ivaneko, Y., Molinari, M., Pisotta, I., Tamburella, F., Labini, F. S., d'Avella, A., der Kooij, H. V., Wang, L., der Helm, F. V., Wang., S., Zanow, F., Hauffe, R., and Thorsteinsson, F., 2012. "Mindwalker: Going one step further with assistive lower limbs exoskeleton for sci condition subjects". In Proceedings of the 4th IEEE RAS/EMBS International Conference on Biomedical Robotics and Biomechatronics.

[10] Aoyagi, D., Ichinose, W. E., Reikensmeyer, D. J., and Bobrow, J. E., 2004. "Human step rehabilitation using a robot attached to the pelvis". In Proceedings of the 2004 ASME International Mechanical Engineering Congress and Exposition, IMECE2004-59472.

[11] Banala, S. K., Agrawal, S. K., and Scholz, J. P., 2007. "Active leg exoskeleton (alex) for gait rehabilitation of motor-impaired patients". In Proceedings of the IEEE 10th International Conference on Rehabilitation Robotics.

[12] Banala, S. K., Kim, S. H., Agrawal, S. K., and Scholz, J. P., 2008. "Assisted gait training with active leg exoskeleton(alex)". In Proceedings of the 2nd Bi-

ennial IEEE/RAS-EMBS International Conference on Biomedical Robotics and Biomechatronics.

[13] Banala, S. K., Kim, S. H., Agrawal, S. K., and Scholz, J. P., 2009. "Assisted gait training with active leg exoskeleton (alex)". *IEEE Transactions on Neural Systems and Rehabilitation Engineering,* **17**(1), February, pp. 2–8.

[14] Emken, J. L., Wayne, J. H., Harkema, S. J., and Reinkensmeyer, D. J., 2006. "A robotic device for manipulating human stepping". *IEEE Transactions on Robotics,* **22**(1), February, pp. 185–189.

[15] Jezernik, S., Colombo, G., Keller, T., Frueh, H., and Morari, M., 2003. "Robotic orthosis lokomat: A rehabilitation and research tool". *International Neuromodulation Society,* **6**(2), pp. 108–115.

[16] Ekkelenkamp, R., Veneman, J., and Kooij, H. V. D., 2005. "Lopes: Selective control of gait functions during the gait rehabilitation of cva patients". In Proceedings of the IEEE 9th International Conference on Rehabilitation Robotics, ThP01-09.

[17] Agrawal, A., Banala, S. K., Agrawal, S. K., and Binder-Macleaod, S. A., 2005. "Design of a two degree-of freedom, ankle-foot orthosis for robotic rehabilitation". In Proceedings of the IEEE 9th International Conference on Rehabilitation Robotics, WeB01-04.

[18] Sawicki, G. S., and Ferris, D. P., 2009. "A pneumatically powered knee-ankle-foot, orthosis (kafo) with myoelectric activation and inihibition". *Journal of Neuro Engineering and Rehabilitation*, June, pp. 6–23.

[19] Kinnaird, C. R., and Ferris, D. P., 2009. "Medial gastrocenmius myoelectric control of a robotic ankle exoskeleton". *IEEE Transactions on Neural Systems and Rehabilitation Engineering,* **17**(1), February, pp. 31–37.

[20] Lockhande, N. G., and Emche, V. B., 2013. "Mechanical spider by using klann mechanisms". *International Journal of Mechanical Engineering and Computer Applications,* **1**(5), October, pp. 13–16.

[21] Komoda, K., and Wagatsuma, H., 2011. "A study of availability and extensibility of theo jansen mechanisms toward climbing over bumps". In Proceedings of the 21st Annual Conference of the Japanese Neural Network Society.

[22] Aan, A., and Heinloo, M., 2014. "Analysis and synthesis of the walking linkage of theo jansen with a flywheel". *Agronomy Research,* **12**(2), pp. 657–662.

[23] Brown, B. C., 2006. "Design of a single-degree-of-freedom biped walking mechanism". *Undergraduate Honors Thesis, The Ohio State University*.

[24] Batayneh, W., Al-Araidah, O., and Malkawi, S., 2013. "Biomimetic design of a single dof stephenson iii leg mechanism". *Mechanical Engineering Research,* **3**(2), July, pp. 43–50.

[25] Angeles, J., and Lopez-Cajun, C. S., 1991. *Optimization of Cam Mechanisms*. Springer Science.

[26] Unruh, V., and Krishnaswami, P., 1995. "A computer-aided design technique for semi-automated infinite point coupler curve synthesis of four-bar linkages". *Journal of Mechanical Design,* **117**, March, pp. 143–149.

[27] McCarthy, J. M., and Soh, G. S., 2010. *Geometric Design of Linkages*, 2nd ed. Springer, New York, USA.

[28] Erdman, A. G., Sandor, G. N., and Kota, S., 2001. *Mechanism Design: Analysis and Synthesis*, fourth edition ed. Prentice-Hall Publ.